P6.7 The Goshen County, Wyoming, supercell of 5 June 2009 intercepted by VORTEX2: Pretornadic phase

PAUL MARKOWSKI,* AND YVETTE RICHARDSON

Department of Meteorology, Pennsylvania State University, University Park, PA

JOSHUA WURMAN, KAREN KOSIBA, AND PAUL ROBINSON

Center for Severe Weather Research, Boulder, Colorado

1. Introduction

This submission is part of a series of presentations in Session 6 dealing with the tornadic supercell intercepted on 5 June 2009 in Goshen County, Wyoming, by the Second Verification of the Origins of Rotation in Tornadoes Experiment (VORTEX2). This preprint supplements a poster summarizing the pretornadic phase of the storm (2100–2148 UTC; tornadogenesis occurred at 2152 UTC). Oral presentations by the same authors will cover the genesis and intensification of the tornado (2248–2202 UTC; paper 6.4), the time during which a relatively steady tornado was observed (2202–2212 UTC; paper 6.5), and the demise of the tornado (2212–2230 UTC; paper 6.6).

Prior to 2130 UTC, the analysis relies on single-Doppler radar data from the Cheyenne, Wyoming, WSR-88D (KCYS). The KCYS radar was approximately 70 km south-southwest of the storm from 2100–2130 UTC (Fig. 1). During the 2130–2142 UTC period, the analysis relies on single-Doppler radar data from the Doppler On Wheels 7 (DOW7) radar obtained from approximately 25–35 km east of the mesocyclone, as well as long-baseline (69 km), dual-Doppler wind retrievals using the KCYS and DOW7 radars. The lowest grid level having a significant region of intersecting beams was 1.2 km AGL. Although vertical velocities could not be accurately retrieved given the degree of extrapolation required to apply the lower boundary condition in the upward-integration of the continuity equation, the influence of the vertical velocity on the retrieval of the horizontal winds in the lowest few kilometers of the storm (at least at these relatively long ranges) is pretty small given the small elevation angles of the radar beam. DOW6 began scanning from a location 15.4 km south-southwest of DOW7 at 2142 UTC, after which time we rely on dual-Doppler wind retrievals from the DOW6-DOW7 pair. We also present mobile mesonet analyses of the virtual potential temperature (θ_v) and equivalent potential temperature (θ_e) fields in the 2140–2148 UTC period (the mobile mesonet probes only reached the mesocyclone region of the storm at approximately 2145 UTC period).

**Corresponding author address*: Dr. Paul Markowski, Department of Meteorology, Pennsylvania State University, 503 Walker Building, University Park, PA 16802; *e-mail*: `pmarkowski@psu.edu`.

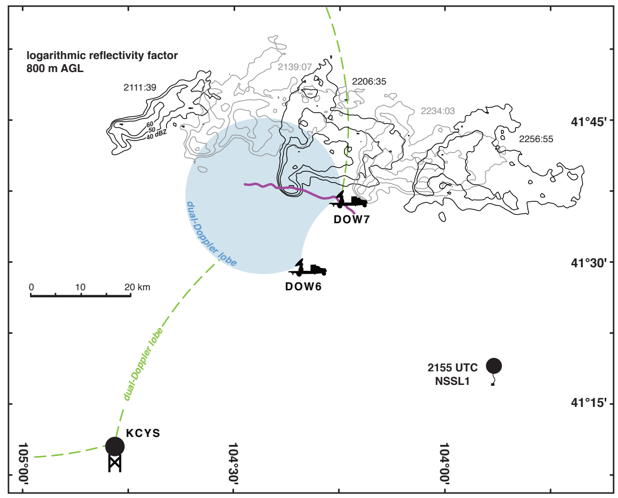

FIG. 1. Large-scale depiction of the track of the Goshen County storm on 5 June 2009 relative to the KCYS, DOW6, and DOW7 radars (the tornado track is purple). Dual-Doppler lobes also are shown.

2. Evolution of the Goshen County storm: 2100–2148 UTC

The Goshen County storm developed from a cluster of cells that was initiated north of Cheyenne shortly after 2000 UTC. By 2105 UTC, the storm had begun to acquire supercell characteristics (e.g., a reflectivity appendage at low levels and cyclonic azimuthal wind shear aloft). Azimuthal wind shear gradually increased from 2105 UTC to the time of the first dual-Doppler wind synthesis at 2130 UTC. This wind synthesis revealed the familiar presence of arching vortex lines (Straka et al. 2007; Markowski et al. 2008) in the vicinity of the center of low-level rotation (nominally 1.2–1.6 km AGL at these early analysis times), whereas vortex lines passing through the midlevel (nominally 6 km AGL) mesocyclone extended into the environment to the south of the storm (i.e., the environmental vortex lines pointed toward the north, which is consistent with the environmental wind profile as revealed by mobile soundings) (Fig. 2).

During the 2140–2144 UTC period, a descending reflectivity core (DRC; Rasmussen et al. 2006; Kennedy et al. 2007; Byko et al. 2009) was detected 4–6 km AGL by the KCYS, DOW6, and DOW7 radars (Fig. 3). Curiously, the DRC was optically invisible in video shot by the Lyndon State photogrammetry team from the location of DOW7, which perhaps suggests that the enhanced reflectivity was the result of a few sparse hailstones. There was a slight suggestion of cloud erosion to the southwest of the wall cloud during this time period, however, perhaps signifying an intensification of the rear-flank downdraft or the development of an occlusion downdraft.

The DRC reached the surface during the 2146–2148 UTC period [we do not wish to be overly specific about a time owing to its dependence on the choice of reflectivity isosurface, and because the nearest radar (DOW7) could not sample below $\sim$400 m]. During this same time period, low-level angular momentum increased markedly relative to earlier times; e.g., at 2148 UTC the circulation about the axis of rotation was nearly 1.4×10^5 m^2 s^{-1} at a radius of 2 km and altitude of 500 m. The increase in circulation was associated with a "surge" of northerly (and later, northwesterly) momentum west of the circulation center, first apparent in the dual-Doppler wind retrievals at 2146 UTC (Fig. 3). The momentum surge was preceded (in space) by a convergence line that has been referred to as a secondary gust front in prior studies (e.g., Wurman et al. 2007, 2011; Marquis et al. 2008). By this stage, the vast majority of vortex lines in the vicinity of the circulation center formed a vertical column that extended out of the top of the data domain (the apexes of the arches were perhaps too high for to be observed, or perhaps by the time the arches were lifted to such high altitudes, their configurations had been significantly modified by additional baroclinic effects or turbulence, the latter of which can cause vortex lines to be severed and reattached to other lines instantaneously as long as there are no loose ends at any time). Tornadogenesis followed shortly thereafter at 2152 UTC.

During the aforementioned period of rotation intensification, mobile mesonet observations were obtained in the forward flank precipitation region and across the hook echo, roughly 5 km north of the circulation center (Fig. 4). The vehicle transects detected θ_v (θ_e) deficits of approximately 4 K (5 K) in the hook echo north of the circulation center, and larger deficits farther north in the core ($>$6 K and $>$10 K, respectively). Observations nearer to the circulation center, and especially to its rear and south, were not obtained until closer to 2200 UTC (thus, we have no in situ thermodynamic observations in the region of the radar-detected DRC). These observations, which will be discussed in the presentations of papers 6.4–6.6, suggest that the air in the near-mesocyclone region was not exceptionally cold during the time the tornado was intensifying, although we cannot easily assess the contribution of hydrometeors to the buoyancy field.

3. Looking ahead

The analysis of this case is far from complete. In the upcoming months, we will further investigate the relationship between the low-level momentum surge that preceded tornadogenesis, and the DRC that was observed aloft prior to the low-level momentum surge (we are careful not to assign cause-and-effect at this point). This includes evaluating the influence of the DRC on the vortex lines in its vicinity, as well as its influence on the angular momentum of the low-level mesocyclone. We also will explore the possible presence of changes in the midlevel wind field that might have been associated with the formation of the DRC. The pursuit of these threads might well require a data assimilation approach, given the challenges in observing the storm's rear flank at midlevels early in the deployment period, as well as the contamination of the near-ground wind field in the mesocyclone region 10–15 minutes prior to tornadogenesis.

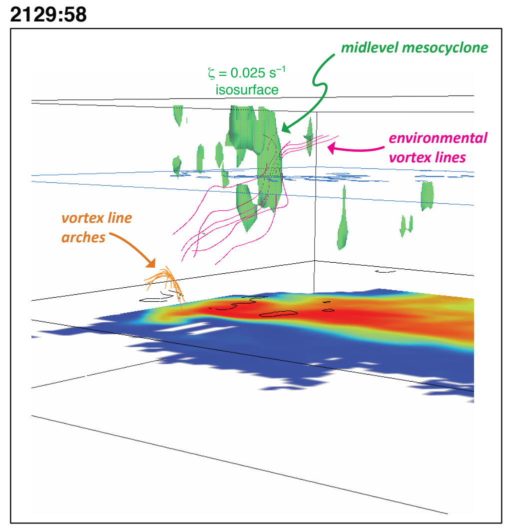

FIG. 2. Vortex lines passing through the midlevel mesocyclone and developing low-level mesocyclone at 2129:58 UTC derived from a dual-Doppler wind synthesis using the KCYS and DOW7 radar data. The 0.025 s^{-1} vertical vorticity isosurface also is shown (green), as is a horizontal cross-section of reflectivity at 1.6 km AGL observed by KCYS. The KCYS and DOW7 data were objectively analyzed to a Cartesian grid having a horizontal and vertical grid spacing of 400 m. A two-pass Barnes weight function was used, with a smoothing parameter on the first pass of $\kappa_0 = 0.66$ km^2. On the second pass, the smoothing parameter was reduced to 30% of its first-pass value. Horizontal scales less than roughly 1.2 km are not well observed at this range from the radars and are therefore strongly suppressed in the analysis.

Acknowledgments. We are grateful for the support of VORTEX2 by the National Science Foundation and National Oceanic and Atmospheric Administration. The authors were supported by awards AGS-0801035 and AGS-0801041 made to PSU and CSWR, respectively. We also thank the countless number of VORTEX2 participants, without which the project would not have been possible. The DOW radars are NSF Lower Atmospheric Observing Facilities supported by NSF-AGS-0734001.

REFERENCES

Byko, Z., P. Markowski, Y. Richardson, J. Wurman, and E. Adlerman, 2009: Descending reflectivity cores in supercell thunderstorms observed by mobile radars and in a high-resolution numerical simulation. *Wea. Forecasting*, **24**, 155–186.

Kennedy, A. D., J. M. Straka, and E. N. Rasmussen, 2007: A statistical study of the association of DRCs with supercells and tornadoes. *Wea. Forecasting*, **22**, 1192–1199.

Markowski, P. M., J. M. Straka, E. N. Rasmussen, R. P. Davies-Jones, Y. Richardson, and J. Trapp, 2008: Vortex lines within low-level

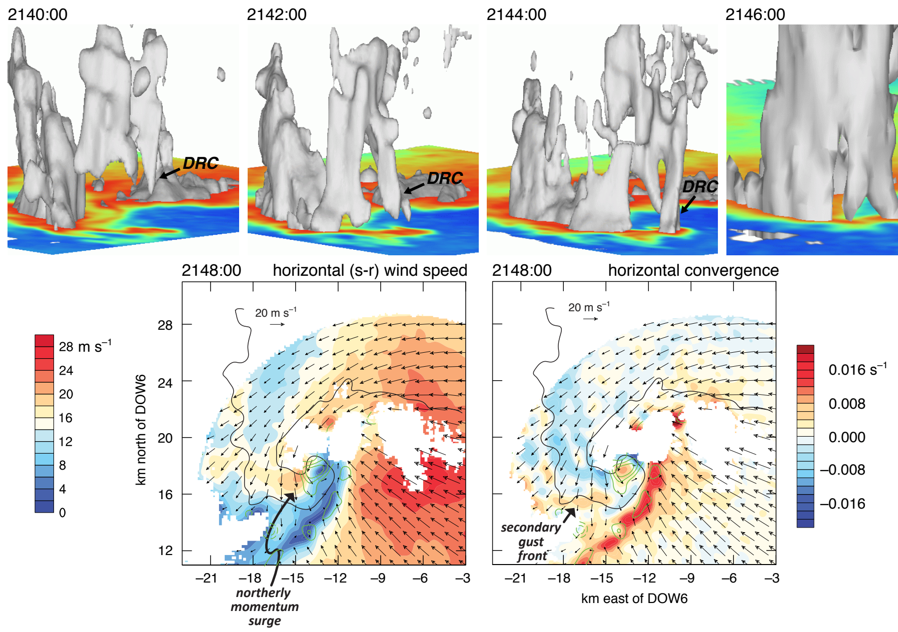

FIG. 3. (Top) Evolution of the 55 dBZ isosurface (DOW7 data) as viewed from the southwest between 2140–2146 UTC. (Bottom) Dual-Doppler-derived horizontal wind fields at 500 m AGL at 2148 UTC: (left) storm-relative wind speed and (right) horizontal convergence. The radar echo is outlined in black, and isovorts are drawn every ± 0.01 s^{-1} in green. The DOW6 and DOW7 data were objectively analyzed to a Cartesian grid having a horizontal and vertical grid spacing of 100 m. A two-pass Barnes weight function was used, with a smoothing parameter on the first pass of $\kappa_0 = 0.28$ km^2. On the second pass, the smoothing parameter was reduced to 30% of its first-pass value. Horizontal scales less than roughly 0.8 km are not well observed at this range from the radars and are therefore strongly suppressed in the analysis.

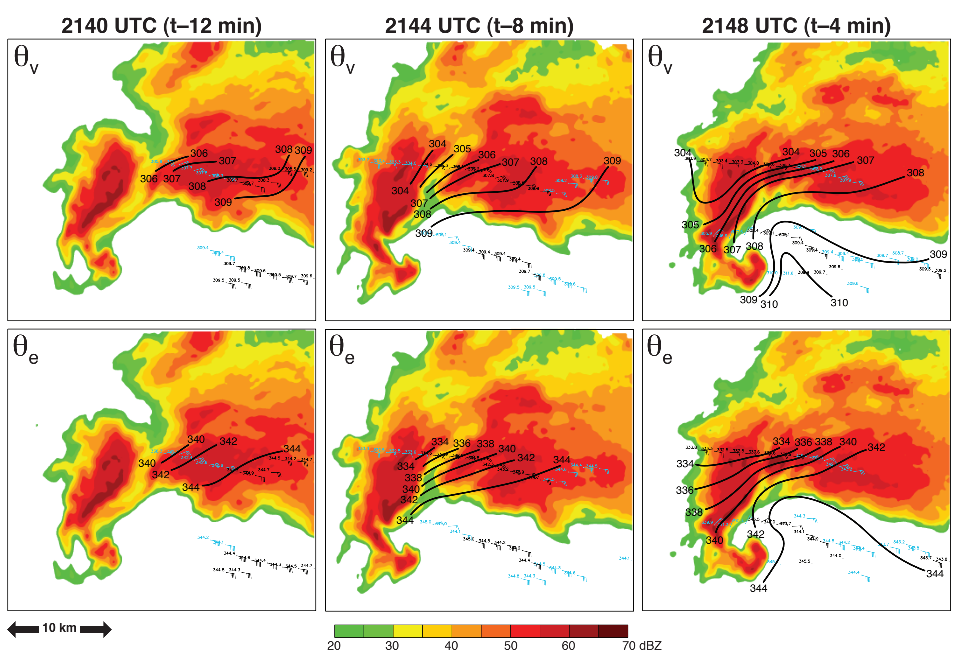

FIG. 4. Manual analyses of θ_v and θ_e derived from mobile mesonet observations. The time-to-space conversion used to create the analyses assumed a steady-state for a 10-min period centered on the analysis time. Observations falling outside of a 5-min window centered on the analysis time are colored light blue.

mesocyclones obtained from pseudo-dual-Doppler radar observations. *Mon. Wea. Rev.*, **136**, 3513–3535.

Marquis, J. M., Y. Richardson, J. Wurman, and P. M. Markowski, 2008: Single- and dual-Doppler analysis of a tornadic vortex and surrounding storm-scale flow in the Crowell, TX, supercell of 30 April 2000. *Mon. Wea. Rev.*, **136**, 5017–5043.

Straka, J. M., E. N. Rasmussen, R. P. Davies-Jones, and P. M. Markowski, 2007: An observational and idealized numerical examination of low-level counter-rotating vortices toward the rear flank of supercells. *E. J. Severe Storms Met.*, **2**(8), 1–22.

Rasmussen, E. N., J. M. Straka, M. S. Gilmore, and R. Davies-Jones, 2006: A preliminary survey of rear-flank descending reflectivity cores in supercell storms. *Wea. Forecasting*, **21**, 923–938.

Wurman, J., Y. Richardson, C. Alexander, S. Weygandt, and P. F. Zhang, 2007a: Dual-Doppler and single-Doppler analysis of a tornadic storm undergoing mergers and repeated tornadogenesis. *Mon. Wea. Rev.*, **135**, 736–758.

Wurman, J., K. Kosiba, P. Markowski, Y. Richardson, D. Dowell, and P. Robinson, 2011: Fine-scale single- and dual-Doppler analysis of tornado intensification, maintenance, and dissipation in the Orleans, Nebraska, supercell. *Mon. Wea. Rev.*, **139**, in press.